Targeted Delivery of Tumor Suppressor MicroRNA-34a to Neuroblastoma Tumors Using Disialoganglioside GD_2 Conjugated to Mesoporous Silica Nanoparticles

Amanda Tivnan[1,2¥], Shannon Orr[3¥], Vladimir Gubala[5], Robert Nooney[5], Suzanne Prenter[1,2], Harry Harvey[1,2], Raquel Domingo Fernández[1,2], Cathy Ng[3], Holger N. Lode[6], David E. Williams[5], Collette McDonagh[5], Andrew M. Davidoff[3,4], Raymond L. Stallings[1,2].

[1]Department of Cancer Genetics, Royal College of Surgeons in Ireland, York House, York Street, Dublin 2, Ireland

[2]National Children's Research Centre, Our Lady's Children's Hospital, Crumlin, Dublin 12, Ireland

[3]Department of Surgery, St. Jude Children's Research Hospital, Memphis, TN 38105, USA

[4]Department of Surgery, University of Tennessee Health Science Center, Memphis, TN 38105, USA

[5]Biomedical Diagnostics Institute, Dublin City University, Glasnevin, Dublin 9, Ireland

[6]Department of Paediatrics and Paediatric Haematology/Oncology, University of Greifswald, Ferdinand-Sauerbruchstrasse, 17475 Greifswald, Germany

[¥] These authors contributed equally to the work and are considered co-first authors.

Contact Information

Raymond L. Stallings rstallings@rcsi.ie Tel: 353 1 402-8533 Fax: 353 1 402-2453

Paragraph (200 words allowed, at 196)

The targeted delivery of a therapeutic directly to tumor cells *in vivo* is of immense importance in the treatment of cancer, as most current cancer therapies have deleterious effects on healthy organ systems. The development of alternative therapies, such as those based on replacement of a tumor suppressive miRNA, are equally important given the relative ease at which many cancers develop multi-drug resistant phenotypes. Here, we demonstrate the first nanoparticle-based targeted delivery of a tumor suppressive microRNA, miR-34a[1-4], to neuroblastoma tumors in a murine orthotopic xenograft model[5]. Neuroblastoma is often a treatment-refractory paediatric cancer originating from precursor cells of the sympathetic nervous system[6], with tumors expressing high levels of the cell surface antigen disialoganglioside GD2 (GD_2). Mesoporous silica nanoparticles conjugated to a chimeric GD_2 antibody (GD_2-Ab ch14.18) and encapsulating mature miR-34a sequences permitted tumor-specific endocytosis following systemic administration to the mouse model. Intra-cellular release of miR-34a resulted in the induction of caspase-mediated apoptosis through targeting of numerous genes associated with cell proliferation and apoptosis and a significant decrease in tumor growth. These novel findings highlight the potential of GD_2-nanoparticle-mediated specific delivery of miR-34a and other therapeutics to neuroblastoma and potentially other GD_2-expressing tumors of neuroectodermal origin.

Main body

Neuroblastoma is the most common extra cranial tumor in childhood, displaying extreme heterogeneity in clinical behaviour, ranging from spontaneous tumor regression to development of a high degree of resistance to standard chemotherapeutic treatments and fatality. MicroRNAs (miRNAs), which negatively regulate gene expression at a post-transcriptional level, are highly associated with aggressive disease pathogenesis and represent potential novel therapeutic targets[7-9]. In this regard, a number of miRNAs are known to induce apoptosis or differentiation when ectopically over-expressed in neuroblastoma cells[4,10-11]. Although miRNA mediated therapeutics has been the subject of many reviews[12], the successful application of miRNAs as a cancer therapy *in vivo* is limited[13-17]. Here, we demonstrate the targeted delivery of miR-34a to neuroblastoma tumors using a disialoganglioside GD2 (GD_2)-antibody conjugated to the surface of nanoparticles systemically administered to a murine orthotopic xenograft disease model.

GD_2 is a galactose-containing cerebroside found on the cell surface membrane of central nervous system tissue that is highly expressed on the cell surface of several human cancers[18], providing a potential target for immunotherapy[19-21,22] and a possible mechanism for targeted delivery of therapeutics. Development of a human/mouse chimeric GD_2 antibody (ch14:18) led to reduction of immunogenicity in patients[23-25]. Although use of GD_2-Ab ch14.18 as a targeting antibody for liposome-mediated therapeutic delivery has previously been evaluated in an *in vitro* model[26], the main disadvantage of standard liposome formulations *in vivo* is their rapid uptake by the reticuloendothelial system, primarily in the liver. In this study, we evaluated mesoporous silica-based nanoparticles[27] which are considered a more stable and inert delivery vehicle.

The use of GD_2 conjugated nanoparticles as a stable system for targeted delivery of miR-34a was extensively evaluated by *in vitro* studies prior to use in a published murine orthotopic

xenograft model of neuroblastoma[5]. The *in vivo* model utilizes two cell lines which stably express luciferase, NB1691 (MYCN amplified) and SK-N-AS (non-MYCN amplified). Both of these cell lines, along with a negative control cell line, HEK293 (embryonic kidney origin), were initially assessed by fluorescence activated cell sorting for GD_2 expression. FACS analysis indicated that GD_2 expression was significantly higher in the two neuroblastoma cell lines relative to HEK293 (**Fig. 1a-c**). In order to determine if GD_2 conjugated nanoparticles would be taken up by GD_2 expressing cells at greater specificity than GD_2 negative cells, NB1691 and HEK293 were treated with different concentrations of GD_2 conjugated nanoparticles tagged with a FITC fluorochrome reporter. Four hours after treatment, cells were washed and FITC fluorescence was measured using a Viktor Microplate luminometer. At concentrations of $6.8x10^9$ particles/ml, uptake was approximately 7.6 fold higher in NB1691 cells relative to HEK293 (normalised to non-coated FITC-doped nanoparticle) (**Fig. 1d**). Notably, higher concentrations of GD_2-FITC-NPs saturated both NB1691 and HEK293 cells, indicating that specificity was dependent upon the concentration of GD_2-FITC-NPs.

In order to evaluate whether miRNAs encapsulated within nanoparticles would be released into the cellular cytoplasm after endocytotic uptake, we constructed GD_2-conjugated nanoparticles encapsulating either miR-34a or a scrambled negative oligonucleotide. Treatment of NB1691, SK-N-AS and HEK293 cells *in vitro* with $6.8x10^9$ particles/ml resulted in a significant up-regulation of miR-34a in the neuroblastoma cell lines, but not in HEK293, (**Fig. 1e**) indicating targeted delivery and release of the nanoparticle contents to GD_2 expressing cells. Moreover, the release of miR-34a in NB1691 and SK-N-AS cells resulted in a significant increase in caspase 3/7 activation (**Fig. 1f** $p<0.05$) and a decrease in cell viability, as determined by both an acid phosphatase assay (**Fig. 1g-h** $p<0.001$) and cell counting (**Supplementary Fig. 1**). No apoptotic response was detected for HEK293 cells, due to the specificity of the GD_2-NPs for GD_2 expressing cells. To confirm that HEK293 cells are

susceptible to miR-34a induced apoptosis, miR-34a was introduced into these cells using a reverse transfection method (**Supplementary Fig. 2**). We also determined that other cell lines of non-malignant origin, such as IMR-90 fibroblasts are also adversely affected by miR-34a (**Supplementary Fig. 3**), providing a rationale for the development of a system for targeted delivery *in vivo*.

Given that our *in vitro* studies indicated that a final concentration of $6.8x10^9$ particles/ml resulted in specific delivery to GD_2 expressing cells and an apoptotic response, a similar initial concentration was used for *in vivo* analysis ($3.4x10^{10}$ particles/mouse provides an estimated $6.8x10^9$ particles/ml based on the assumption that an average mouse (20g) possesses a circulating blood volume of 1.2ml or 60ml/kg[28]). FITC-GD_2-NPs were systemically administered to tumor bearing mice at day 14, after tumor establishment had been verified. The mean fluorescence intensities of tumors were 6.7 to 258 fold greater than in healthy organs (liver, spleen, kidney, lung and heart) scanned *ex vivo* (**Fig. 2b**). Among the normal organs, FITC signal was highest in liver, which could potentially be due to the detoxification function of this organ. The mean fluorescence intensity of tumors from mice injected with FITC-GD_2-NPs was 13.85 fold higher (**Fig. 2c** $p<0.05$) than tumors from mice injected with FITC-nanoparticles lacking GD_2, further confirming targeted delivery.

Given the success of our *in vivo* targeting experiments, we then evaluated GD_2-coated nanoparticles as a means of targeted delivery of miR-34a as a potential therapeutic to neuroblastoma tumors using the $NB1691^{luc}$ and $SK\text{-}N\text{-}AS^{luc}$ orthotopic xenograft models. Both $NB1691^{luc}$ and $SK\text{-}N\text{-}AS^{luc}$ tumor bearing mice were systemically administered either GD_2-miR-34a-NP or GD_2-miRneg-NP (containing a scrambled oligonucleotide) at day 14, 17 and 20 post-tumor establishment. Ultra-sonography and bioluminescence analysis, prior to nanoparticle injection (day 13 post-tumor induction), indicated equivalency of tumor sizes in miR-34a versus negative control treated populations (**Supplementary Fig. 4**). Tumors were

then monitored on days 18, 21 and 25 by bioluminescent imaging (**Fig. 3a-d**). Bioluminescent intensity in both NB1691^{luc} and SK-N-AS^{luc} tumor bearing mice injected with GD_2-miR34a-NP was significantly reduced relative to mice injected with GD_2-miRneg-NP ($p<0.05$ for both tumor types). Measurements of post-mortem tumor volumes and weights (day 25) confirmed the highly significant reduction in tumor growth in GD_2-miR34a-NP treated mice (**Supplementary Fig. 5**).

Notably, enhanced miR-34a levels were detected by qPCR in NB1691^{luc} and SK-N-AS^{luc} tumors treated with GD_2-miR34a-NP relative to those treated with GD_2-miRneg-NP (**Fig. 3e,f**; respectively,$p<0.05$ and $p<0.001$). Interestingly, two of the SK-N-AS^{luc} tumors exhibited no increase in miR-34a levels, and these two tumors correspond to two outlier tumors (**Fig. 3d**) which grew somewhat faster than the main tumor cohort, the most likely explanation being that one or more of the tail vein injections failed on these two mice.

qPCR analysis also indicated a significant decrease in mRNA levels for the validated miR-34a target oncogene, *MYCN* in the NB169^{luc} tumors (*MYCN* amplified) (**Fig. 3g** $p<0.001$). Although not statistically significant, there was also a trend towards *MYCN* reduction in the non-*MYCN* amplified SK-N-AS^{luc} tumors (**Fig. 3h**). The decreased MYCN mRNA in NB1691^{luc} tumors was further validated at protein level by western blot (Figures 3i and j). TUNEL staining of paraffin embedded tumor sections showed significantly increased apoptosis in both NB1691^{luc} and SK-N-AS^{luc} tumors treated with GD_2-miR34a-NP relative to GD_2-miRneg-NP (**Fig. 4a-c**). Immunohistochemical staining of tumor sections with other markers, notably, CD34 (a marker of vascularisation) and KI67 (proliferation) displayed a significant reduction in vascular endothelial cells (**Fig. 4d-f**) and results for KI67 (**Fig. 4g-i**); respectively.

Evaluation of non-specific delivery of miR-34a to normal organs was paramount to ensuring specific targeting of the GD_2-NPs to the neuroblastoma tumor. In this regard, liver,

kidneys and lungs were assessed for possible increases in endogenous levels of miR-34a after treatment with GD_2-miR34a-NPs. All organs assessed did not exhibit any significant increase in mature miR-34a transcript levels subsequent to treatment, relative to GD_2-miRneg-NP treated controls (**Supplemental Fig. 6**). Blood chemistries were analysed in GD_2-miRneg-NP and GD_2-miR34a-NP-treated animals to evaluate the effects, if any, administration of mesoporous silica nanoparticles might have on the animal. From the data analysed (**Supplementary Fig. 7**) systemic tail vein injection of either miR-negative control or miR-34a–GD_2-nanoparticles did not appear to cause significant adverse effects on kidney and/or liver function.

Recently, non-targeted lipid based delivery of miR-34a was shown to have anti-tumorigenic effects on a mouse xenograft model of prostate cancer, with the authors suggesting that the miR-34a formulation was successfully tolerated by mice[29]. Targeting of miRNA therapeutics, however, could be of far greater importance in humans with longer life spans, and especially as a potential therapeutic for children with developing organs. Here, we have shown that over-expression of miR-34a in cell lines of non-malignant origin causes significant apoptosis, and one might expect this miRNA to have similar adverse effects on proliferating healthy cells *in vivo*. The efficacy with which GD_2-NP-mediated delivery of miR-34a significantly hinders tumor progression, in both $NB1691^{luc}$ and $SK\text{-}N\text{-}AS^{luc}$ murine tumor models, provides evidence for the potential use of miRNA-mediated therapeutics in neuroblastoma and potentially other cancers, such as melanoma or small cell lung carcinoma, that express high levels of the surface antigen GD_2.

Acknowledgements

This work was supported in part by Science Foundation Ireland Principal Investigator Award (07/IN.1/B1776) (RLS), the Children's Medical and Research Foundation (RLS), the

Assisi Foundation of Memphis (AMD), the US Public Health Service Childhood Solid Tumor Program Project Grant No. CA23099 (AMD), the Cancer Center Support Grant No. 21766 from the National Cancer Institute (AMD), and by the American Lebanese Syrian Associated Charities (ALSAC) (AMD). Dr. Christopher Calabrese and staff of the Small Animal Imaging facility; and all technicians and staff associated with Department of Surgery, St. Jude Children's Research Hospital, Memphis, TN 38105, USA**.**

Author Contributions

AT and SO carried out all laboratory work pertaining to this study, participated in its design and drafted the final manuscript. VG, RN, DW and CMcD were involved in the nanoparticle formulation and bioconjugation of GD2-Ab ch14.18 to nanoparticle preparations. HL provided the GD2-Ab ch14.18 antibody for use in this study. AMD provided expertise on *in vivo* neuroblastoma modelling and access to animal facilities in St. Jude Children's Research Hospital, Memphis, TN. CN carried out FACS analysis on cell lines for GD_2 expression. SP, RF and HH were involved in tumor and organ RNA and protein isolation, Western Blotting and qPCR analysis of miR-34a target transcripts. RLS and AMD conceived the study, and participated in its design and coordination and helped to draft the manuscript. All authors read and approved the final manuscript.

Figure Legends

Figure 1 *In vitro* analysis of GD_2 conjugated nanoparticles. **(a)** FACS analysis, using a GD_2 primary antibody and goat anti-mouse IgG2a-PE secondary antibody indicated little, if any, GD_2 surface antigen on HEK293 cells. Conversely NB1691 **(b)** and SK-N-AS **(c)** cells showed significant GD_2 reactivity. **(d)** Varying concentrations of FITC-GD_2-NPs were added to cell culture media of NB1691 or HEK293 ($1x10^6$ cells). A concentration of $6.8x10^9$

particles/ml was found to be the optimal dosage tested for specific delivery of FITC fluorophore to NB1691 neuroblastoma cells with minimal incorporation into HEK293 cells. **(e)** GD_2-miR34a-NPs treatment led to ~2 fold increase in miR-34a levels in NB1691 cells, ~30 fold increase in SK-N-AS cells (* $p<0.05$, n=3), with no significant change in miR-34a transcript levels in HEK293 cells. **(f)** NB1691 and SK-N-AS cells showed a significant increase in caspase 3/7 activity relative to GD_2-miRneg-NP-treated cells after 72 hrs (*$p<0.05$, n=3) while HEK293 cells showed no significant increase in caspase activity under these conditions. Acid phosphatase assays indicated a significant reduction in viable cell numbers for **(g)** NB1691 and **(h)** SK-N-AS cells treated with GD_2-miR34a-NPs ($6.8x10^9$ particles/ml), over a 96 hour period (***$p<0.001$) relative to GD_2-miRneg-NP-treated controls. **(i)** HEK293 cells showed no significant reduction of viable cells following treatment with GD_2-miR34a-NP ($p>0.05$, n=3).

Figure 2 Demonstration of tumor specific targeting by systemically administered GD_2 conjugated nanoparticles tagged with FITC. **(a)** Systemic administration through lateral tail injection of FITC-GD_2-NPs ($3.4x10^{10}$ particles/200µl) resulted in targeted delivery of FITC dye predominantly to tumors (indicated by fluorescence intensity color map generated from scans using IVIS instrumentation). **(b)** FITC-GD_2-NP-treated organs have significantly less fluorescence than isolated tumors (*$p<0.05$, n=4-5) and **(c)** FITC-GD_2-NP treated tumors showed significantly greater presence of FITC dye relative to FITC-NP treated tumors (*$p<0.05$, n=4-5).

Figure 3 *In vivo* analysis of GD_2 conjugated nanoparticles bearing miR-34a or negative control oligonucleotide. Bioluminescent images representative of mice bearing **(a)** $NB1691^{luc}$ tumors treated with GD_2-miRneg-NP (left) or GD_2-miR34a-NP (right), along with

representative mice bearing **(b)** SK-N-AS^{luc} tumors treated with GD_2-miRneg-NP (left) or GD_2-miR34a-NP (right) were obtained at day 25. Tumor growth curves from **(c)** mice bearing NB1691^{luc} tumors treated with GD_2-miRneg-NP (black line) or GD_2-miR34a-NP (red line) and **(d)** mice bearing SK-N-AS^{luc} tumors treated with GD_2-miRneg-NP (black line) or GD_2-miR34a-NP (red line). Time points for systemic administration of nanoparticles are indicated by the symbol ▲. Differences in tumor growth between mice injected with GD_2-miR34a-NP versus GD_2-miRneg-NP were statistically significant for both models (NB1691^{luc} n=8, *p<0.05) (SK-N-AS^{luc} *p<0.05 for n=8 and **p<0.01 for n=6). For the SK-N-AS^{luc} model, two tumors grew significantly faster than the median, potentially indicating failure of one or more tail vein injections. Mature miR-34a transcript levels were significantly higher in GD_2-miR34a-NP treated tumours relative to GD_2-miRneg-NP-treated control tumors in both the **(e)** NB1691^{luc} (***p<0.001, n=8) and **(f)** SK-N-AS^{luc} (*p<0.05, n=8). **(g)** MYCN, a validated target of miR-34a, mRNA levels were significantly reduced in GD2-miR34a-NP treated NB1691^{luc} tumors relative to negative controls (**p<0.001, n=8) **(h)** qPCR of SK-N-AS^{luc} tumors showed a trend in reduction of MYCN expression **(i)** MYCN reduction in NB1691^{luc} was validated at a protein level by Western Blot and **(j)** protein suppression was quantified using densitometry.

Figure 4 Analysis of tumors treated with miR-34a and negative control oligonucleotides. TUNEL staining was carried out on paraffin embedded section of SK-N-AS^{luc} **(a)** and NB1691^{luc} **(b)** tumors. In both tumor subtypes, treatment with GD_2-miR34a-NPs led to a significant increase in apoptosis (**c**, ***p<0.0001, n=8). Immunohistochemistry staining with CD34 showed a marked decrease in the endothelial cell marker subsequent to GD_2-miR34a-NP treatment (**d-f**, ***p<0.0001, n=8). KI67 staining showed…(**4g-i**)…

Methods

Cell Lines. NB1691 and SK-N-AS cells were maintained in RPMI-1640 supplemented with heat-inactivated foetal bovine serum (FBS, 10%) and l-glutamine (1%). NB1691^{luc} and SK-N-AS^{luc} cell lines were also supplemented with 100μg/mL Zeocin (InVivoGen, San Diego, California). HEK293 cells were grown in DMEM supplemented with FBS (10%) and l-glutamine (1%). Each cell line was validated by aCGH profiling for identification of previously published genomic abnormalities.

Reverse transcription, Real-time qPCR and Western Blotting. Total RNA was extracted using a miRNeasy© kit (Qiagen Inc, Valencia, CA). Reverse transcription was carried out using 50ng of total RNA with a primer specific for miR-34a, or random primers for gene expression, and the TaqMan reverse transcription kit (Applied Biosystems). qPCR was carried out on the 7900 HT Fast Real-time System (Applied Biosystems). β-actin, was used for normalization. A relative fold change in expression of target miRNA/gene transcripts was determined using the comparative cycle threshold method ($2^{-\Delta\Delta CT}$). Total protein was isolated from cells using a radioimmunoprecipitation assay (RIPA) lysis buffer (Sigma-Aldrich Corp., St. Louis, MO). Protein concentration was measured using the BCA assay from Millipore. Proteins were fractionated on 10% polyacrylamide gels and blotted onto nitrocellulose membrane. The membrane was probed with Anti-MYCN antibody (n-mycn: Santa Cruz (SC-53993), 1:500) or anti α-tubulin (Abcam (AB7291), 1:5000 used for loading controls). Signal was detected using Immoblion Western (Millipore) and densitometry was determined using the ImageJ processing program[30].

Fluorescence Activated Sorting Analysis. Log phase cells ($2x10^6$) were harvested and stained with GD_2 primary antibody (Santa Cruz, sc-53831) and a goat anti-mouse IgG2a-PE secondary antibody (Santa Cruz, sc-3738). Cells were then collected ($1x10^3$) and analyzed by FACS Calibur (BD Bioscience).

Synthesis of FITC dye doped silica nanoparticle; empty or containing either miR-34a or a miR-negative control: All chemicals were obtained from Sigma Aldrich, (Sigma-Aldrich Corp., St. Louis, MO) unless otherwise stated. Silica nanoparticles containing fluorescein (3 (w/w)) and synthetic premiR-34a (0.1 (w/w)), or a scrambled miR-negative control (0.1 (w/w)), were prepared using a microemulsion method[31].

Conjugation of GD_2-Ab ch14.18 to the nanoparticles. Conjugation was performed in duplicate for nanoparticles containing miR-34a or a miR-negative control, according to a previously published protocol using PAMAM dendrimers[32]. The NP–antibody bioconjugates were aliquoted (0.1mg) and later re-suspended in sterile cell culture media immediately prior to use. In parallel, FITC-only doped GD_2-NPs were also synthesized using the aforementioned protocol.

MicroRNA and nanoparticle treatment of NBL cells in vitro. The Pre-miR™ to miR-34a (30μM) and the premiR-negative control miRNA (negative control 1, Applied Biosystems) were reverse transfected into NB1691, SK-N-AS and HEK293 cell lines using the transfection agent siPORT™ NeoFX™ (Applied Biosystems/Ambion, Austin, TX). For nanoparticle experiments, NB1691, SK-N-AS and HEK293 cell lines were seeded at the required confluency 24 hours prior to treatment. Each vial of freeze-dried nanoparticles ($1.7x10^{11}$ particles) was resuspended in pre-warmed cell culture media (1ml) and protected from the light (stock solution of nanoparticles $1.7x10^{11}$ particles/ml). The final concentration used was $6.8x10^{9}$ particles/ml.

Fluorescence analysis. Following treatment with FITC doped nanoparticles, cells were lyzed using a RIPA buffer and centrifuged at 14,000rpm for 15 minutes at 4°C. The relative fluorescent units (RFUs) of isolated supernatant (50μl) was then detected using a Viktor Microplate luminometer (Molecular Devices, Sunnyvale, CA).

Acid phosphatase assays. Cells were transfected in 96-well plates ($1x10^4$ cells per well). At designated time points post-treatment, cells were washed with PBS and 10mM *p*-nitrophenol phosphate in sodium acetate (0.1M) with triton X-100 (0.1%) being added. Plates were incubated at 37°C for two hours in the dark and the reaction was stopped with sodium hydroxide (50µl 1M) per well. Absorbance was measured at 405nm.

Caspase 3/7 activity assay. NB1691, SK-N-AS and HEK293 cells were plated in quadruplicate in 96-well plates. 72 hours after nanoparticle treatment or miRNA transfection, caspase activity was measured using the 3/7 Caspase detection kit from Promega (Madison, WI) in accordance with manufacturers protocols. Luminescence was read on a Viktor Microplate luminometer (Molecular Devices, Sunnyvale, CA).

***In vivo* targeting and nanoparticle delivery.** All animal experiments were carried out using CB-17/SCID mice (Charles' River Laboratories, Wilmington, MA) and were performed in accordance with a protocol approved by the Institutional Animal Care and Use Committee of St Jude Children's Research Hospital, Memphis, Tennessee. Retroperitoneal tumors were established by injection of $2x10^6$ $NB1691^{luc}$ or $SK\text{-}N\text{-}AS^{luc}$ cells behind the left adrenal gland via a left subcostal incision under administration of isoflurane (2%), and tumors were allowed to develop over 13 days (n=8 per cohort). $3.4x10^{10}$ nanoparticles/mouse (either fluorophore-doped-GD_2-coated NPs, fluorophore-doped-NPs, GD_2-miR34a-NPs, or GD_2-miRneg-NPs-treated) were administered via lateral tail vein injection to mice with pre-established retroperitoneal neuroblastoma (day 21 for the targeting experiments with FITC doped nanoparticles; day 13 for the microRNAs bearing nanoparticles. Scanning of resected tumours and organs *ex vivo* or of tumors *in vivo* was performed using an IVIS Imaging System 100 Series (Xenogen Corporation, Alameda, CA). For experiments using nanoparticles bearing miR-34a or a negative control oligonucleotide, animals in each cohort were tumor size matched using ultrasound and bioluminescent imaging, and each cohort received repeat

injections with GD_2-miRneg-NPs or GD_2-miR34a-NPs ($3.4x10^{10}$ particles/mouse) at 3 day intervals (days 14, 17 and 20 post-tumor induction). For imaging, mice received an intraperitoneal injection of D-Luciferin (150-mg/kg, Caliper Life Sciences, Hopkinton, MA).

Tumor Immunohistochemistry. Formalin-fixed, paraffin-embedded, 4-μm thick tumor sections were stained with rat antimouse CD34 antibody (RAM 34; PharMingen, San Diego, Calif) or KI67 (CAT no.). TUNEL staining was carried out in accordance with previously published protocols[33] and all images were analysed using an Olympus U-SPT microscope as previously described[34].

Statistical analysis. The Mann-Whitney non-parametric, one-tailed unpaired test was used to analyze significance of change in tumor bioluminescence over time, post-mortem tumour analysis of miR-34a expression by qPCR, mean cell viability, caspase activation and cell numbers at final time points in individual experiments (all data is plotted as the median + standard error of the mean).

Abbreviations. Quantitative PCR (*qPCR*), Fluorescein 5(6)-isothiocyanate*(FITC)*; aminopropyltrimethoxysilane *(APTMS)*; tetraethylorthosilicate*(TEOS)*; 3-(Trihydroxysilyl)propyl methylphosphonate, monosodium salt solution *(THPMP)*; Poly-amidoamine *(PAMAM)*; 1-Ethyl-3-[3-dimethylaminopropyl] carbodiimide hydrochloride *(EDC)*; N-hydroxysulfosuccinimide *(sulfo-NHS)*; 2-(N-morpholino)ethanesulfonic acid *(MES)*

References

1. **Cole, K.A., *et al.* A functional screen identifies miR-34a as a candidate neuroblastoma tumor suppressor gene. *Mol Cancer Res* 6, 735-742 (2008).**
2. **Tivnan, A., *et al.* MicroRNA-34a is a potent tumor suppressor molecule in vivo in neuroblastoma. *BMC Cancer* 11, 33 (2011).**
3. **Wei, J.S., *et al.* The MYCN oncogene is a direct target of miR-34a. *Oncogene* 27, 5204-5213 (2008).**
4. **Welch, C., Chen, Y. & Stallings, R.L. MicroRNA-34a functions as a potential tumor suppressor by inducing apoptosis in neuroblastoma cells. *Oncogene* 26, 5017-5022 (2007).**

5. **Dickson, P.V.*, et al.* In vivo bioluminescence imaging for early detection and monitoring of disease progression in a murine model of neuroblastoma. *J Pediatr Surg* 42, 1172-1179 (2007).**
6. **Wagner, L.M. & Danks, M.K. New therapeutic targets for the treatment of high-risk neuroblastoma. *J Cell Biochem* 107, 46-57 (2009).**
7. **Bray, I.*, et al.* Widespread dysregulation of MiRNAs by MYCN amplification and chromosomal imbalances in neuroblastoma: association of miRNA expression with survival. *PLoS One* 4, e7850 (2009).**
8. **Buckley, P.G.*, et al.* Chromosomal and microRNA expression patterns reveal biologically distinct subgroups of 11q- neuroblastoma. *Clin Cancer Res* 16, 2971-2978 (2010).**
9. **Chen, Y. & Stallings, R.L. Differential patterns of microRNA expression in neuroblastoma are correlated with prognosis, differentiation, and apoptosis. *Cancer Res* 67, 976-983 (2007).**
10. **Das, S.*, et al.* MicroRNA mediates DNA demethylation events triggered by retinoic acid during neuroblastoma cell differentiation. *Cancer Res* 70, 7874-7881 (2010).**
11. **Foley, N.H.*, et al.* MicroRNA-184 inhibits neuroblastoma cell survival through targeting the serine/threonine kinase AKT2. *Mol Cancer* 9, 83 (2010).**
12. **Bader, A.G., Brown, D. & Winkler, M. The promise of microRNA replacement therapy. *Cancer Res* 70, 7027-7030 (2010).**
13. **Esquela-Kerscher, A.*, et al.* The let-7 microRNA reduces tumor growth in mouse models of lung cancer. *Cell Cycle* 7, 759-764 (2008).**
14. **Kota, J.*, et al.* Therapeutic microRNA delivery suppresses tumorigenesis in a murine liver cancer model. *Cell* 137, 1005-1017 (2009).**
15. **Liu, C.*, et al.* The microRNA miR-34a inhibits prostate cancer stem cells and metastasis by directly repressing CD44. *Nat Med* 17, 211-215.**
16. **Trang, P.*, et al.* Systemic Delivery of Tumor Suppressor microRNA Mimics Using a Neutral Lipid Emulsion Inhibits Lung Tumors in Mice. *Mol Ther*.**
17. **Wiggins, J.F.*, et al.* Development of a lung cancer therapeutic based on the tumor suppressor microRNA-34. *Cancer Res* 70, 5923-5930.**
18. **Ritter, G. & Livingston, P.O. Ganglioside antigens expressed by human cancer cells. *Semin Cancer Biol* 2, 401-409 (1991).**
19. **Handgretinger, R.*, et al.* A phase I study of human/mouse chimeric antiganglioside GD2 antibody ch14.18 in patients with neuroblastoma. *Eur J Cancer* 31A, 261-267 (1995).**
20. **Yu, A.L.*, et al.* Phase I trial of a human-mouse chimeric anti-disialoganglioside monoclonal antibody ch14.18 in patients with refractory neuroblastoma and osteosarcoma. *J Clin Oncol* 16, 2169-2180 (1998).**
21. **Zeytin, H.E., Tripathi, P.K., Bhattacharya-Chatterjee, M., Foon, K.A. & Chatterjee, S.K. Construction and characterization of DNA vaccines encoding the single-chain variable fragment of the anti-idiotype antibody 1A7 mimicking the tumor-associated antigen disialoganglioside GD2. *Cancer Gene Ther* 7, 1426-1436 (2000).**
22. **Lode, H.N.*, et al.* Targeted interleukin-2 therapy for spontaneous neuroblastoma metastases to bone marrow. *J Natl Cancer Inst* 89, 1586-1594 (1997).**
23. **Mueller, B.M., Romerdahl, C.A., Gillies, S.D. & Reisfeld, R.A. Enhancement of antibody-dependent cytotoxicity with a chimeric anti-GD2 antibody. *J Immunol* 144, 1382-1386 (1990).**

24. **Zeng, Y.*, et al.* Anti-neuroblastoma effect of ch14.18 antibody produced in CHO cells is mediated by NK-cells in mice. *Mol Immunol* 42, 1311-1319 (2005).**

25. **Forster-Waldl, E.*, et al.* Isolation and structural analysis of peptide mimotopes for the disialoganglioside GD2, a neuroblastoma tumor antigen. *Mol Immunol* 42, 319-325 (2005).**

26. **Pagnan, G.*, et al.* Delivery of c-myb antisense oligodeoxynucleotides to human neuroblastoma cells via disialoganglioside GD(2)-targeted immunoliposomes: antitumor effects. *J Natl Cancer Inst* 92, 253-261 (2000).**

27. **Gubala, V., Le Guevel, X., Nooney, R., Williams, D.E. & MacCraith, B. A comparison of mono and multivalent linkers and their effect on the colloidal stability of nanoparticle and immunoassays performance. *Talanta* 81, 1833-1839 (2010).**

28. **Wolfensohn, S. & Lloyd, M. *Handbook of Laboratory Animal Management and Welfare*, (Blackwell Publishing, 2003).**

29. **Liu, C.*, et al.* The microRNA miR-34a inhibits prostate cancer stem cells and metastasis by directly repressing CD44. *Nat Med* 17, 211-215 (2011).**

30. **Abramoff, M.D., Magelhaes, P.J. & Ram, S.J. Image Processingwith ImageJ. *Biophotonics International* 11, 36-42 (2004).**

31. **Nooney, R.I.*, et al.* Experimental and theoretical studies of the optimisation of fluorescence from near-infrared dye-doped silica nanoparticles. *Anal Bioanal Chem* 393, 1143-1149 (2009).**

32. **Gubala, V.*, et al.* Kinetics of immunoassays with particles as labels: effect of antibody coupling using dendrimers as linkers. *Analyst* Advance Article(2011).**

33. **Sims, T.L.*, et al.* IFN-beta restricts tumor growth and sensitizes alveolar rhabdomyosarcoma to ionizing radiation. *Mol Cancer Ther* 9, 761-771 (2010).**

34. **Williams, R.F.*, et al.* Targeting multiple angiogenic pathways for the treatment of neuroblastoma. *J Pediatr Surg* 45, 1103-1109 (2010).**

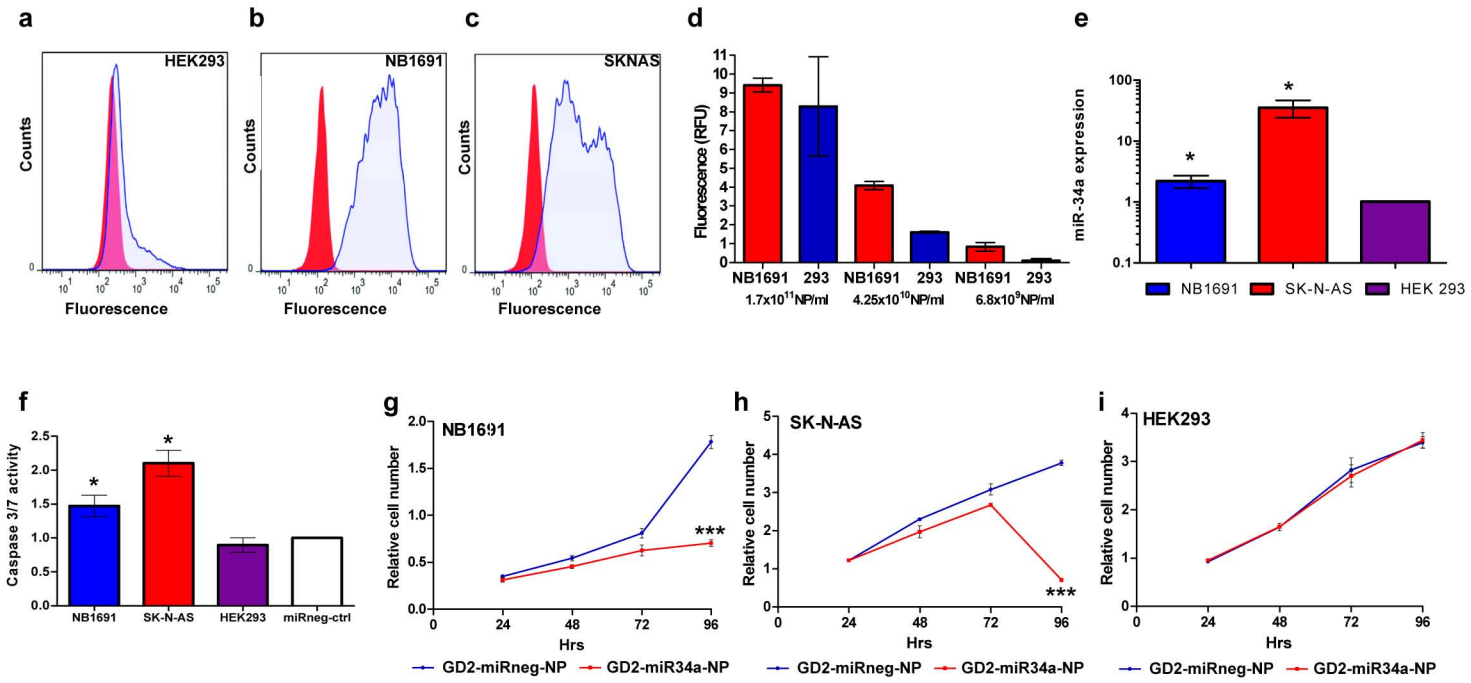
a
HEK293
Counts
Fluorescence
b
NB1691
Counts
Fluorescence
c
SKNAS
Counts
Fluorescence
d
Fluorescence (RFU)
NB1691
293
NB1691
293
NB1691
293
1.7x10^11 NP/ml
4.25x10^10 NP/ml
6.8x10^9 NP/ml
e
miR-34a expression
NB1691
SK-N-AS
HEK 293
f
Caspase 3/7 activity
NB1691
SK-N-AS
HEK293
miRneg-ctrl
g
NB1691
Relative cell number
Hrs
GD2-miRneg-NP
GD2-miR34a-NP
h
SK-N-AS
Relative cell number
Hrs
GD2-miRneg-NP
GD2-miR34a-NP
i
HEK293
Relative cell number
Hrs
GD2-miRneg-NP
GD2-miR34a-NP

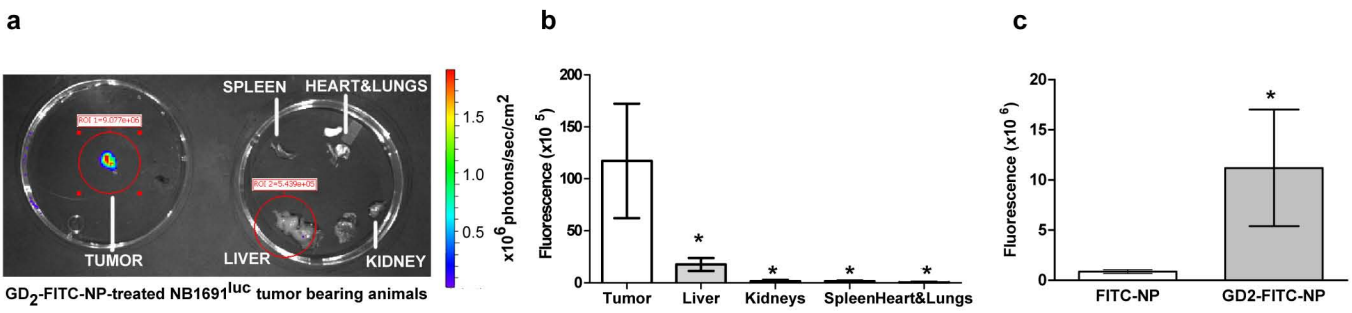
a
SPLEEN
HEART&LUNGS
TUMOR
LIVER
KIDNEY
1.5
1.0
0.5
x10^6 photons/sec/cm^2
GD2-FITC-NP-treated NB1691luc tumor bearing animals
b
Fluorescence (x10^5)
200
150
100
50
0
Tumor
Liver
Kidneys
SpleenHeart&Lungs
c
Fluorescence (x10^6)
20
15
10
5
0
FITC-NP
GD2-FITC-NP

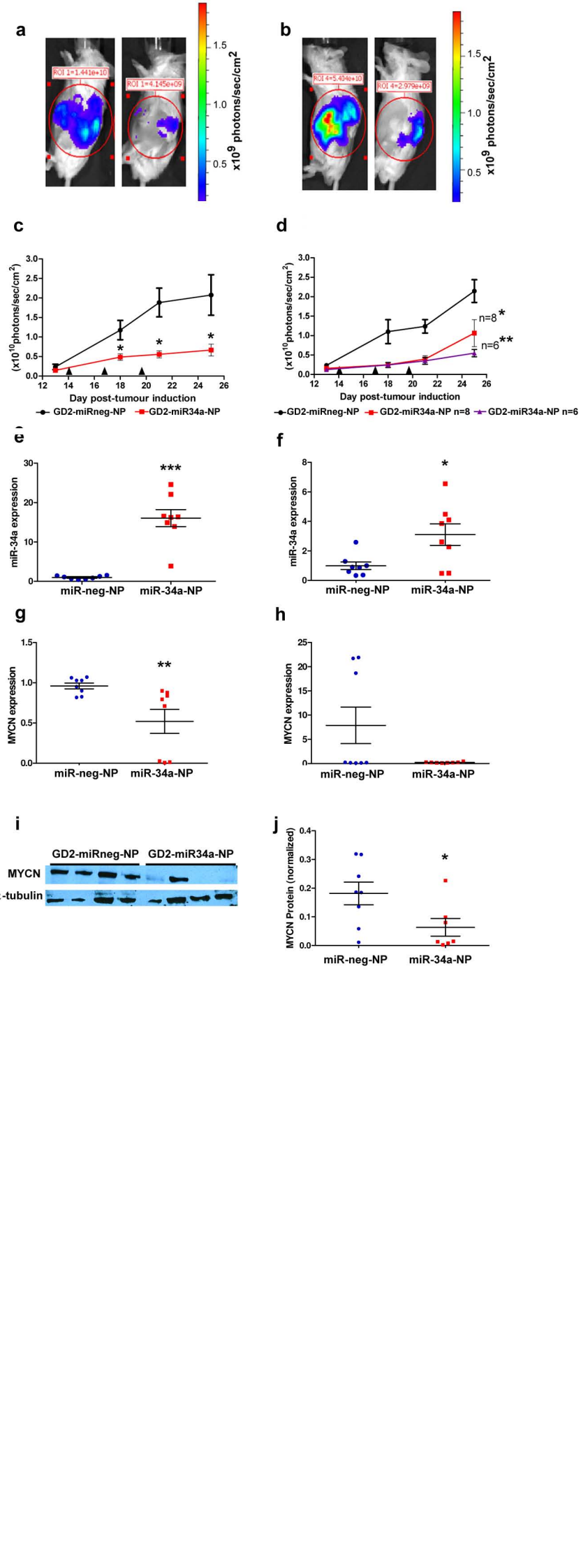
a
ROI 1=1.441e+10
ROI 1=4.145e+09
1.5
1.0
0.5
x10^9 photons/sec/cm^2
b
ROI 4=5.404e+10
ROI 4=2.979e+09
1.5
1.0
0.5
x10^9 photons/sec/cm^2
c
(x10^10photons/sec/cm^2)
Day post-tumour induction
GD2-miRneg-NP
GD2-miR34a-NP
d
(x10^10photons/sec/cm^2)
n=8 *
n=6 **
Day post-tumour induction
GD2-miRneg-NP
GD2-miR34a-NP n=8
GD2-miR34a-NP n=6
e
miR-34a expression
***
miR-neg-NP
miR-34a-NP
f
miR-34a expression
*
miR-neg-NP
miR-34a-NP
g
MYCN expression
**
miR-neg-NP
miR-34a-NP
h
MYCN expression
miR-neg-NP
miR-34a-NP
i
GD2-miRneg-NP
GD2-miR34a-NP
MYCN
α-tubulin
j
MYCN Protein (normalized)
*
miR-neg-NP
miR-34a-NP

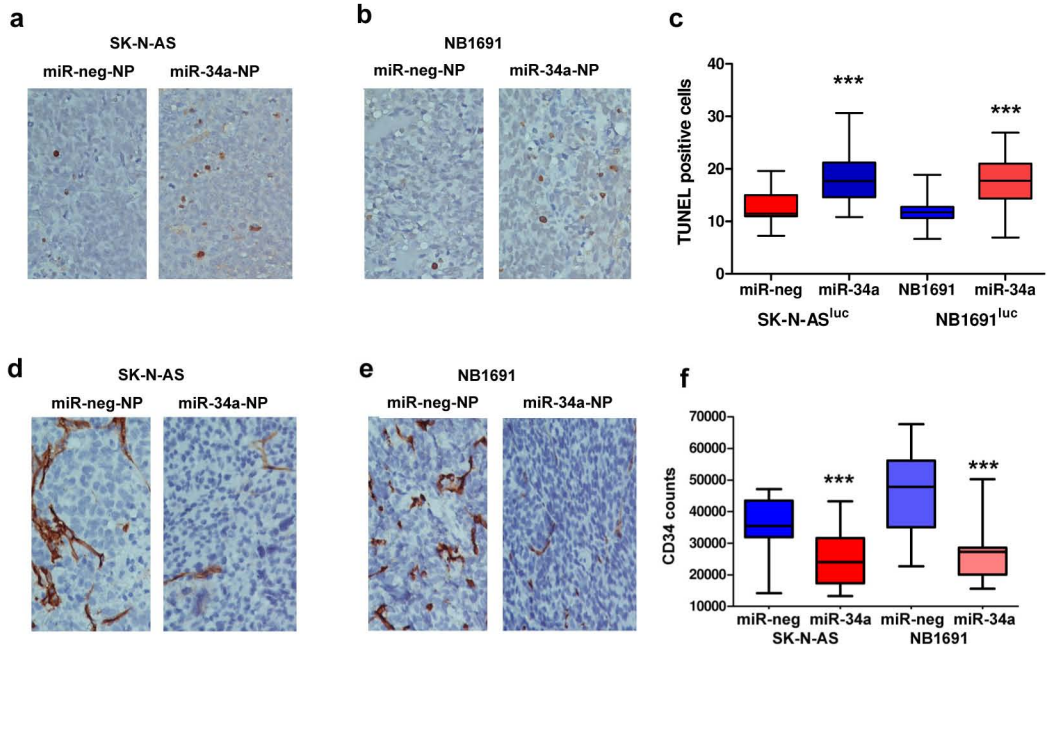
a
SK-N-AS
miR-neg-NP
miR-34a-NP
b
NB1691
miR-neg-NP
miR-34a-NP
c
TUNEL positive cells
40
30
20
10
0
***
***
miR-neg
miR-34a
NB1691
miR-34a
SK-N-AS luc
NB1691 luc
d
SK-N-AS
miR-neg-NP
miR-34a-NP
e
NB1691
miR-neg-NP
miR-34a-NP
f
CD34 counts
70000
60000
50000
40000
30000
20000
10000
***
***
miR-neg
miR-34a
miR-neg
miR-34a
SK-N-AS
NB1691
g
SK-N-AS
miR-neg-NP
miR-34a-NP
h
NB1691
miR-neg-NP
miR-34a-NP
i